LA-UR- 00-3513

Title: **CHARACTERIZATION OF A LARGE-VOLUME, MULTI-ELEMENT CDZNTE DETECTOR**

Author(s): **T. H. Prettyman, M. C. Browne, K. D. Ianakiev, and C. E. Moss**

Submitted to: **SPIE Conference**
San Diego, California

(TECHNICAL PAPER)

Los Alamos
NATIONAL LABORATORY

Form 836 (10/96)

DISCLAIMER

DRAFT: Not for general distribution.
To appear in *Proceedings of SPIE* (2000). Los Alamos National Laboratory document LA-UR-00-XXXX.

Characterization of a Large-Volume, Multi-Element CdZnTe Detector

Thomas H. Prettyman,* Michael C. Browne, Kiril D. Ianakiev, and Calvin E. Moss
Los Alamos National Laboratory, MS E540, Los Alamos, NM 87545

Steven A. Soldner
eV PRODUCTS, Saxonburg, PA 16056

ABSTRACT

In this paper, we present results of experiments to characterize a large-volume (4 cm^3), multi-element CdZnTe detector for high-efficiency, gamma-ray spectroscopy. The module includes an array of eight 0.5 cm^3 coplanar grid detectors manufactured by eV Products. An eight-channel data acquisition system with list mode output is used to record gamma ray events for each detector in the array. The list mode data are analyzed to determine the efficiency for coincidence events and to demonstrate different modes of operation (e.g. Compton suppression). The total efficiency of the array is found to match Monte Carlo calculations to within a few percent; however, the full-energy (photopeak) efficiency is significantly lower than predicted by Monte Carlo. The observed difference is probably caused by a combination of electrode design and charge transport properties. Approaches to improve full-energy efficiency are proposed.

Keywords: CdZnTe, coplanar grid, room temperature, semiconductor, gamma ray detectors, spectroscopy, safeguards

1. INTRODUCTION

CdZnTe is a compound semiconductor material that is being developed for use in portable measurement applications and remote sensing. The high resistivity of CdZnTe enables it to be used for gamma ray spectroscopy over a wide range of ambient temperatures (-20°C to 40°C). Active cooling is not required. Consequently, compact, low-power detectors can be manufactured. In addition, the pulse height resolution that can be achieved by CdZnTe detectors is typically much better than the resolution of scintillation detectors. Consequently, CdZnTe is being implemented for applications for which the use of intrinsic germanium is cumbersome (due to the size and weight of the equipment and logistical considerations such as liquid nitrogen handling) and for which the resolution of scintillation detectors such as NaI(Tl) and CsI(Tl) is inadequate. We are developing CdZnTe for applications ranging from *in situ* nondestructive assay of nuclear material to planetary science.

CdZnTe is grown commercially by the Bridgman-Stockbarger method. The principal US supplier (eV Products) primarily uses high-pressure vertical Bridgman (HPVB) furnaces to grow the material. Other variants of the Bridgman method are being explored. However, HPVB is presently the main source of material and is capable of reliably producing high-resistivity material with electron transport properties needed for spectroscopy.

The main limitation of CdZnTe technology is the size of single crystals that can be routinely harvested from ingots grown by HPVB. Grain boundaries are known to trap electrons and, if included within a detector, can reduce the full-energy (photopeak) efficiency and degrade pulse height resolution. Consequently, single crystal material is desired for gamma-ray spectroscopy. At present, the largest single crystals manufactured for gamma-ray spectrometers from HPVB material are on the order of 15 mm × 15 mm × 7.5 mm (~1.7 cm^3). Photographs of slices of the material (Fig. 1) show the range of grain sizes found in HPVB material.

Single crystals provided by the HPVB process are adequate for many applications; however, there are a number of applications in which larger volume is needed. For example, *in situ* identification and assay of plutonium-bearing materials (e.g., holdup measurements and customs inspections) require higher detection efficiency than can currently be provided. CdZnTe is also a candidate for future planetary missions and gamma ray spectrometers are needed for elemental analysis of planetary bodies. CdZnTe detectors are being proposed for Discovery missions to Mercury, comets, and asteroids, and Outer

* Correspondence: Email: thp@lanl.gov; www: http://www.nis5.lanl.gov/; Telephone: 505 667-6449; Fax: 505 665-5910.

Solar System missions (e.g., to the Jovian satellites). The determination of elemental composition requires the detection of gamma rays up to 10 MeV. Single crystal detectors will probably be effective on a lander or a rover since they are placed close to the gamma ray source. However, they will only be useful at relatively low energies (< 2 MeV). In addition, the size of single crystal detectors is well below that needed for an orbiter.

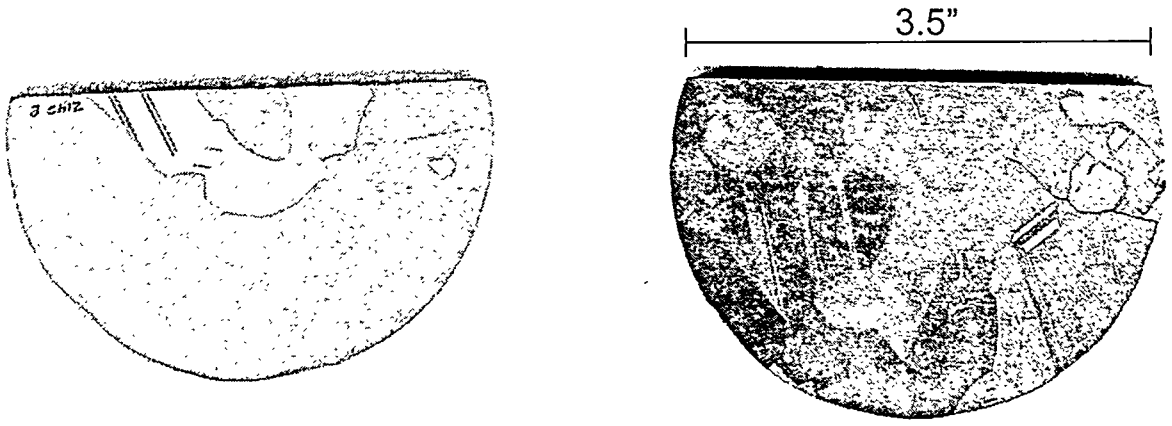

Figure 1. Slices of HPVB material taken perpendicular to the axis of the ingot (Photographs courtesy of eV Products).

2. MULTI-ELEMENT DETECTOR

We are developing techniques to combine multiple single crystals to make high efficiency detectors for portable measurement applications and remote sensing. We are currently focusing on analog electronics for signal combination; however, we have also begun to investigate digital signal processing techniques for large detector arrays. Recently, we developed a multi-element detector, consisting of an array of eight 10 mm × 10 mm × 5 mm coplanar grid detectors. The array was mounted in a hand-held probe that contained all pulse shaping electronics needed to provide a single spectroscopy output to an off-the-shelf, portable multi-channel analyzer (MCA). A detailed description of the CdZnTe detector array and pulse shaping electronics for hand-held operation is given by Prettyman, et al.[1]

A diagram of the hand held detector module is shown in Fig. 2 along with a photograph of the electronics package. The module was designed to include a scintillation detector for use as a high efficiency counter and active shield for background and Compton suppression. The shield is segmented and can be used as a gamma-ray field polarimeter (i.e., to determine the direction of the incident gamma-rays). The target application is emergency response, in which a high efficiency detector is needed to locate special nuclear material and a spectroscopy system is needed for identification.

The module serves as a useful platform for determining the general characteristics of multi-element detectors and electronics. In this paper, we present the results of experiments to characterize the detector array, in which the multi-element module was connected to an eight-channel ADC with a time-tagged, list mode output. The ADC allowed us to determine the attributes of the array, including the detection efficiency for multiple-element interactions, and to study different modes of operation.

A block diagram of the pulse shaping electronics is given in Fig. 3. Each detector is connected to two preamplifiers and a difference circuit, which is the standard configuration for coplanar grid detectors. A linear analog filter was selected for pulse shaping (CR-RC^4 with gated base-line restorer [BLR] and adaptive noise threshold) to ensure adequate integral linearity, wide dynamic range, and minimum threshold for event detection. When the module is used as a hand held detector, the output of the linear analog filter is fed into a summing amplifier that is part of the module. In order to characterize the array, the summing amplifier was replaced by the 8-channel data acquisition system (the component labeled "8-channel ADC" in the block diagram). For hand held operation, the BLR logic pulse is used for signal recognition and controls the gate of the summing amplifier. Variations in carrier collection time cause time jitter between pulses in multiple scattering events that need to be summed. Consequently, a pulse stretcher must follow the output of the linear amplifier. The peak hold circuit shown in Fig. 3 acts as a stretcher.

Bias and low-voltage power was supplied externally by the MCA. An internal divider circuit was used to provide differential bias to the detectors. The power consumption of the multi-element module is given in Table 1. We used standard printed circuit board (PCB) technology with surface mounted components to minimize design costs. With this approach, we were able to design a compact, low-power system. To achieve low power, we used rail-to-rail output designs for all stages of the shaping circuit. In addition, we used low-voltage components (±5V). This resulted in an eight-channel detector than consumed less than 1W. Note that the coplanar grid front end consumes a factor of four less than commercially available electronics. Future designs will be developed with ±3V components, which will reduce the power consumption further.

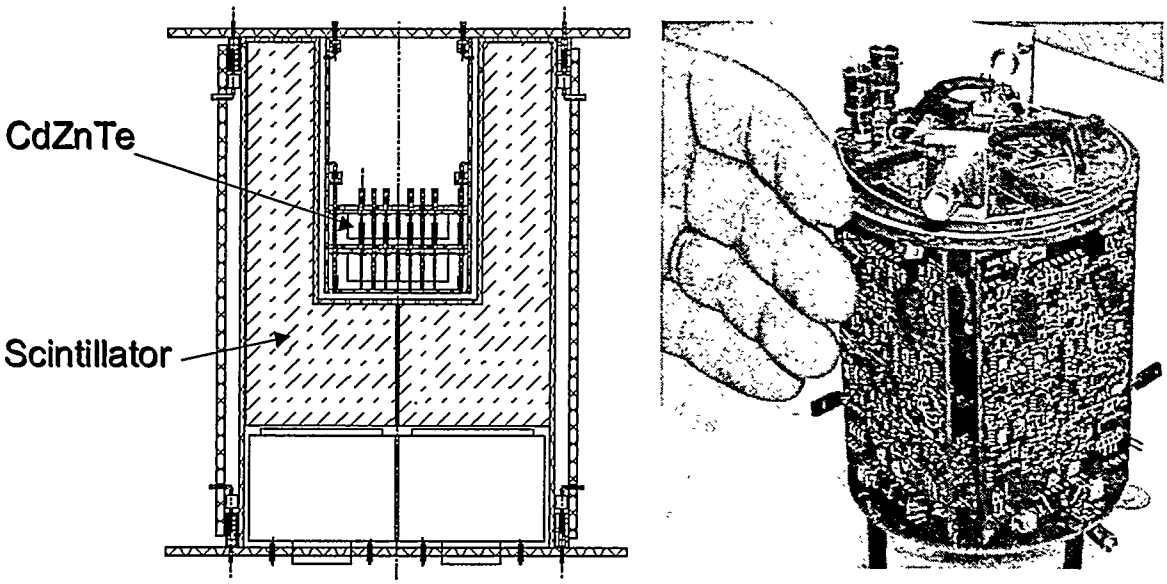

Figure 2. Schematic diagram and photograph of the 8-element detector.

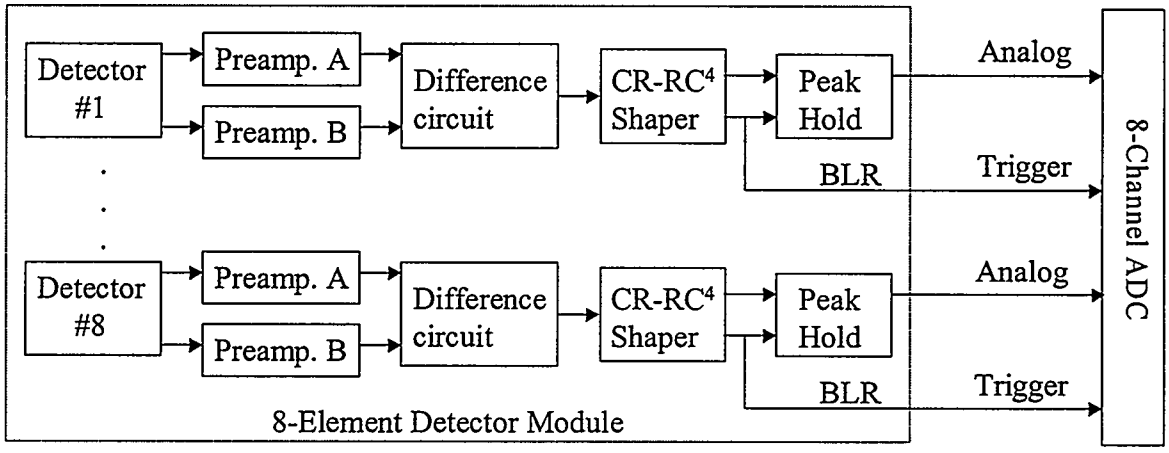

Figure 3. Electronics block diagram

Table 1. Power consumption for the 8-element module.

Component	Supply voltage		Commercially-available product (if available)
	±5V	±3.3V	
Single channel			
Coplanar grid front end (2 preamplifiers and difference circuit)	70 mW	50 mW	~300 mW (+12V hybrid)
Amplifier	40 mW	30 mW	
Stretcher	30 mW	20 mW	
Total	*140 mW*	*95 mW*	
8-element detector			
Summing amplifier	15 mW	10 mW	
Pulse processing	1040 mW	760 mW	
Total	*1055 mW*	*770 mW*	

3. EXPERIMENTAL RESULTS

Data from the 8-element detector was taken with a University of Washington developed data acquisition (DAQ) system. The system incorporates a custom-designed 8-channel 6U VME ADC card that is programmed and controlled via fiber-optic link to the DAQ computer. Additionally, each channel of the ADC card is equipped with a 32-bit time-tag-module with 250-ns resolution (reprogrammable to 50-ns). The 8 channels of the ADC card were modified to accept shaped and stretched analog pulses at the ADC inputs, and were triggered by the base line restorer (BLR) signals from the shaping electronics. The system was operated in an asynchronous mode to allow pulses from each detector in the array to be recorded independently. Data in the form of ADC value, channel, and time for each event were recorded in list-mode for off-line analysis.

An analysis code was developed to provide pulse height spectra and coincidence information for the 8-element detector. The analysis code used full energy peaks from ^{57}Co, ^{137}Cs, and ^{54}Mn sources to provide a linear energy calibration of each ADC channel. List-mode data was normalized to energy and scanned for coincidences by looking for multiple events in a specified time window. A time-between-events histogram was generated from which it was determined that 2 μs was an optimal coincidence window size. Coincidence events were labeled as NHIT=2, 3, 4, or 5 depending on the number of elements fired in a given coincidence window. This was done to prevent double counting of multiply coincident events.

Energy-normalized ADC values were extracted from the data set and recombined to form pulse height spectra. Pulse height spectra were formed for individual detector elements. The pulse height resolution of individual elements was found to range from 20 keV to 36 keV full-width-at-half-maximum (FWHM) at 662 keV. When the module was operated as a hand-held detector, the worst resolution was 23 keV FWHM at 662 keV.[1] We believe that the loss in resolution is caused increased noise due to ground loops between the data acquisition system and detector module. The spectra for individual elements were used to determine the threshold for signal detection, which was found to be ~80 keV.

The data set was used to simulate the gated sum output of the hand-held detector (i.e., pulses are combined only for those elements whose signal exceeds the noise threshold). We also formed the coincidence spectrum, for which signals were combined only when two or more channels received a signal. The Compton continuum in the coincidence spectrum is suppressed because the likelihood of the gamma ray escaping the detector after the second scatter is small (compared to the probability following a single interaction). Consequently, we refer to the coincidence spectrum as the "accepted spectrum." The spectrum corresponding to single interactions is the "rejected spectrum." Figure 4 shows the accepted and rejected spectra for a ^{137}Cs run, and Figure 5 shows these spectra for a ^{60}Co run. Note that the continuum was suppressed in the accepted spectrum.

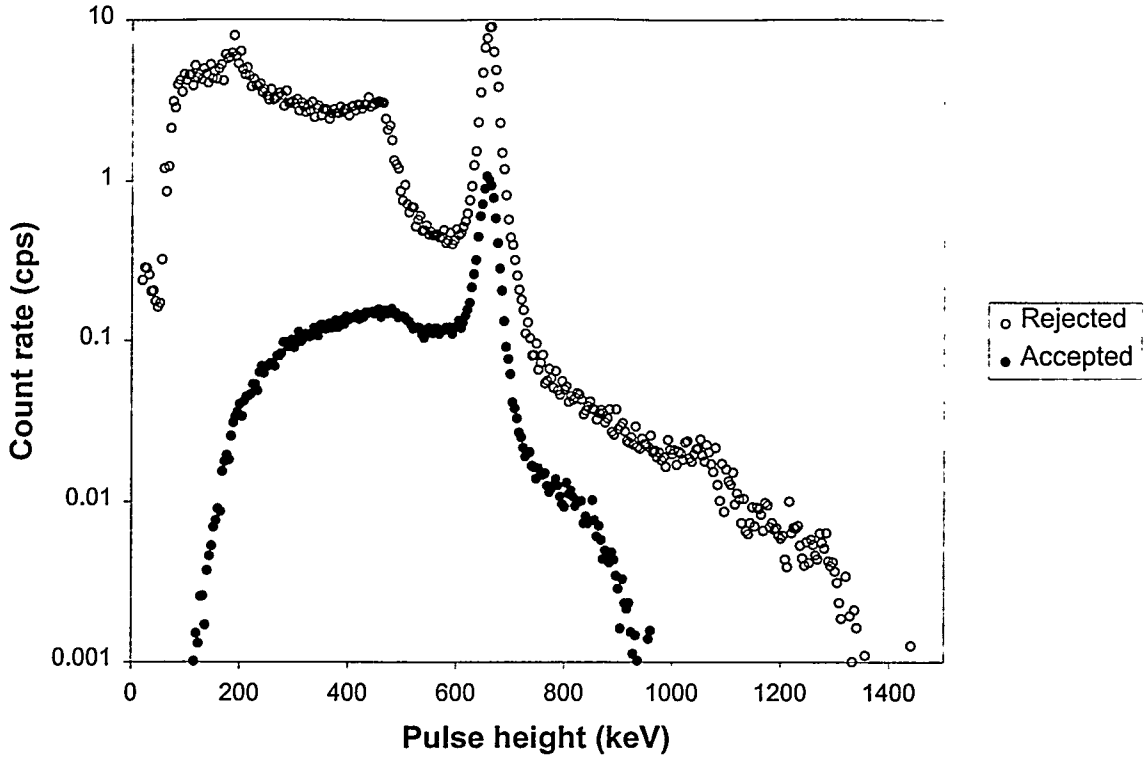

Figure 4. Pulse height spectra for ^{137}Cs.

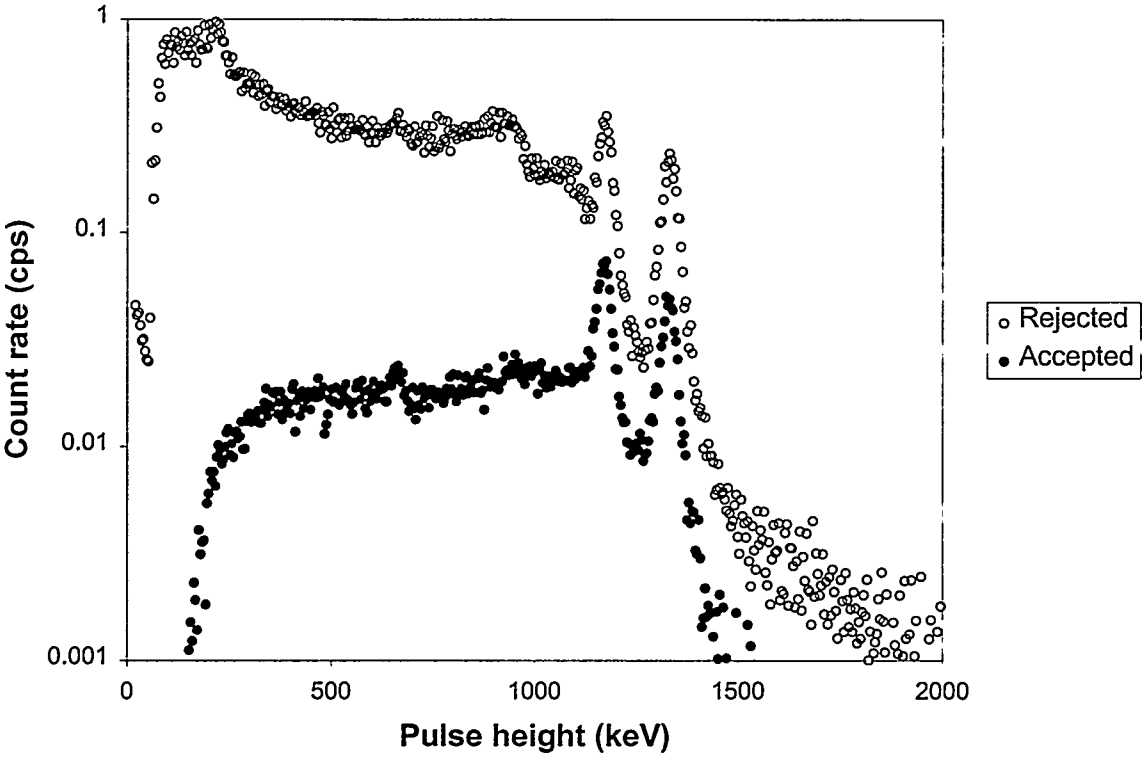

Figure 5. Pulse height spectra for ^{60}Co.

Data from the 8-element detector was also analyzed for "cross-talk". This examines coincidences as a function of physical element position, and only NHIT=2 coincidences were considered in this analysis. Figure 6 shows the layout of the individual elements of the detector, and Figure 7 shows the cross-talk rate for a ^{137}Cs run as a matrix of element position. The source position for the data shown in Figure 7 was 19.8 cm directly above the top 4 elements of the array. Scattered γ rays are primarily forward-biased for incident energies around 662 keV (^{137}Cs), indicating that the number of "straight-through" (*i.e.* 1-5, 2-6, 3-7, and 4-8 coincidences) interactions should dominate the cross-talk matrix. This effect is seen in the data shown in Figure 7, with these straight-through rates ranging from 1.1 to nearly 10 times greater than other coincident configuration rates. Also note that nearly 50% of all coincident configurations show in the cross-talk matrix fall in the full-energy peak.

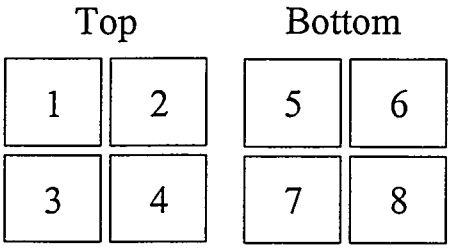

Figure 6. Array layout. Note that detector 1 is directly in front of detector 5 when the array is viewed from the radiation source.

2	3	4	5	6	7	8	
0.437 44.1%	0.522 42.0%	0.148 40.5%	1.63 45.0%	0.527 46.4%	0.533 42.3%	0.137 40.0%	1
	0.178 39.2%	0.486 46.2%	0.490 42.0%	1.50 50.0%	0.256 43.4%	0.258 42.8%	2
		0.424 46.2%	0.589 42.3%	0.254 46.2%	1.72 43.2%	0.248 44.0%	3
			0.245 44.9%	0.484 48.2%	0.551 40.3%	0.740 47.5%	4
				0.675 46.9%	0.420 43.0%	0.089 46.2%	5
					0.248 43.4%	0.283 46.6%	6
						0.295 47.2%	7

Figure 7. Cross-talk matrix for ^{137}Cs. Each cell represents an interaction between two detectors whose indices are given in the uppermost row and rightmost column. The total count rate (counts per second) for events resulting from coincidences is given at the top of each cell. The percentage of all coincident events that appear in the full energy peak is given at the bottom of each cell.

4. MONTE CARLO CALCULATION

A Monte Carlo code was developed to simulate gamma ray transport in arrays of detectors. The geometry of the 8-element module was modeled using a general-geometry-modeling package similar to the one used by MCNP. The model for the 8-element module included the alumina substrate on which the array elements were mounted as well as surrounding materials (PCB, stand, table top, etc.). The Monte Carlo code provided a detailed simulation of gamma ray transport (similar to "full physics" mode for MCNP) and was capable of simulating coincidence spectra produced by the multi-element module. All tallies were given in units of cm^2 so that the flux of gamma-rays incident on the detector could be converted directly to count rate.

The code has a simple "point" model to simulate the resolution of coplanar grid detectors. The model includes lower- and upper-exponential tails and a flat continuum. Parameters for the resolution model can be extracted from the experimental spectra. This feature can be used to predict the performance of the array under realistic measurement conditions. For the calculations presented in this paper, the resolution model was turned off. So, the count rates reported for spectral features are the theoretical maximum. The threshold for signal detection was included in the model. All of the detectors were assigned a threshold of 80 keV.

Data for ^{137}Cs were taken using a 62 μCi source positioned 19.8 cm directly above the array. Attenuation of the 662 keV gamma rays by the intervening printed circuit boards was estimated to be 2%. Neglecting attenuation by intervening materials, the flux of 662 keV gamma rays was 395 $cm^{-2}s^{-1}$. This value was used to scale the Monte Carlo calculation to determine count rate. The flux can also be used to determine detector efficiency from rates quoted in the tables that follow.

Count rates estimated by Monte Carlo are compared to experimental count rates in Table 2. The total count rate is given along with the full energy count rate for each spectrum. The numbered spectra correspond to individual elements. All rates are given in counts per second (cps). Note that the total count rates computed by Monte Carlo are within 3% of the average total count rates for the front and back arrays and the total count rate for the gated sum. However, the computed full-energy count rates are significantly higher than the experimental full-energy rates for all spectra. The experimental full energy count rates for individual elements are ~62% of the count rates predicted by Monte Carlo. Note that the variation in count rates between elements is small: The standard deviation in count rate for the top array is ~3%. The standard deviation in count rate for the bottom array is 4%.

The cross-talk matrix was computed for interactions between detector 1 and all other elements. The results are given in Fig. 8, which can be compared to the first row in the experimental cross talk matrix shown in Fig. 7. The calculated cross talk rates are significantly lower than the experimental rates; however, the calculation shows a similar trend. For example, the "straight-through" cross talk is dominant in both the calculation and experiment.

Table 2. Comparison between experiment and Monte Carlo for ^{137}Cs.

Spectrum	Experiment		Calculation	
	Full energy (cps)	Total (cps)	Full energy (cps)	Total (cps)
1	10	73.4	15.6	71.0
2	9.6	71.3		
3	9.8	67.3		
4	9.4	67.3		
5	7.8	59.0	12.5	60.5
6	8.4	67.3		
7	7.8	61.3		
8	7.6	60.2		
Gated sum	79.9	499	139	485
Rejected	70.3	477	112	445
Accepted	9.5	22.3	26.7	39.4

2	3	4	5	6	7	8	
1.76 74.3%	1.77 75.3%	0.63 71.7%	2.95 67.2%	1.09 60.9%	1.10 62.8%	0.56 58.2%	1

Figure 8. Calculated cross-talk matrix for ^{137}Cs. Each cell represents an interaction between two detectors whose indices are given in the uppermost row and rightmost column. The total count rate (counts per second) for events resulting from coincidences is given at the top of each cell. The percentage of all coincident events that appear in the full energy peak is given at the bottom of each cell.

5. DISCUSSION

The measured full-energy efficiency of the detectors and the array appears to be 40% lower than the maximum theoretical efficiency. One reason for the difference is that the charge measurement efficiency of coplanar grid detectors varies significantly in the near anode region (between 500- and 1000-μm from the anode, depending on their design). This region creates a featureless continuum below the full-energy peak. However, this can account for no more than 20% of the observed difference.

The coplanar grid detectors used in the array were designed and manufactured by eV Products. The grid pattern is similar to the "third generation" pattern described by He.[3] This design includes bus bars to inter-connect grid electrodes, which form interlocking parallel strips. The grid electrodes are extended to wrap around each other to compensate for edge effects in the direction parallel to the strips. A guard ring was included in the pattern to eliminate surface leakage between the cathode and the grid electrodes. In addition, the width of grid electrodes was made narrower than the gaps in order to reduce surface leakage.

We observed charge pulses produced by alpha particles from ^{241}Am (in a flood exposure of the cathode) for a 0.5 cm^3 coplanar grid detector (designated H15-08) with the same grid design used in the array.[4] Under typical bias conditions, charge pulses for the unbiased electrode show no evidence of collection or charge sharing. Experiments with array detectors show that the guard ring also does not collect charge. So, the deficit in efficiency is probably not caused by parasitic collection by the sensing electrode or guard ring.

The material for the detector array was selected from ingot H15 (the same ingot from which H15-08 was manufactured). The average electron mobility-lifetime product for H15 material was ~3×10^{-3} cm^2/V. Only single crystal material was selected for the array (i.e., free from visible grain boundaries, but with the possibility of the inclusion of twins). Given the absence of visible grain boundaries, it is unlikely that electron trapping is responsible for the observed deficit in efficiency. Furthermore, we expect grain boundaries to be included randomly in the crystals. So, the presence of grain boundaries would cause the full-energy efficiency of the array elements to vary considerably. This is inconsistent with the experiment: the full-energy efficiency of the array elements is uniform.

The most plausible reason for the deficit relates to the design of the electrodes, the method used to form the spectroscopy signal, and selection of the material. A study was carried out by Prettyman, et al.[4] on the design, manufacturing and characterization of cylindrical coplanar grid detectors. The efficiency of cylindrical coplanar grid detectors was determined for detectors manufactured from two different ingots (I03 and C26). The full-energy efficiency of the detectors manufactured for ingot I03 were close to the theoretical efficiency; however, the efficiency for detectors manufactured from C26 was low by an amount similar to the deficit observed in this study. The main difference between the two ingots was the electron mobility-lifetime product. Ingot I03 had an average electron mobility lifetime product of 5×10^{-3}. Ingot C26 had an average electron mobility lifetime product of 3×10^{-3}.

Coplanar grid detectors use a gain adjustment in the difference circuit to compensate for electron trapping. However, the gain adjustment is only effective when the weighting potential for the grid electrodes is uniform over the volume of the

detector. This way, the same gain adjustment is valid over the entire volume. If the weighting potential varies laterally over the device, then the optimal gain adjustment will also vary laterally.

With a guard ring design, the weighting potential varies significantly near the edge of the detector. So, the gain adjustment is probably only effective in compensating for electron trapping in the middle of the device. Events that occur near the edge of the detector will not appear in the full energy peak. For material with high mobility lifetime products (such as I03), the gain adjustment is not critical and lateral variations in weighting potential do not result in a loss in efficiency as long as the weighting potential for the biased and grounded electrodes are matched. For material with low mobility lifetime products (such as C26 or H15), lateral variations in the weighting potential cause a significant loss in full-energy efficiency.

6. SUMMARY AND CONCLUSIONS

A list-mode data acquisition was used to acquire data from an eight-element detector module. Compton suppression was demonstrated by analyzing the list mode data and forming a coincidence spectrum. This approach for Compton suppression will be useful for planetary missions, where larger arrays will be used to measure high energy gamma-rays (up to 10 MeV). The data acquisition system was also used to characterize the detector array. Experimental count rates were compared with theoretical count rates for both single elements and coincidences. Results show that the full-energy efficiency of individual elements is much lower than the maximum theoretical values. While more research is needed to determine the source of the problem, our preliminary conclusion is that the deficit in efficiency is caused by the selection of material with low electron mobility-lifetime products. For future arrays, material with higher mobility lifetime products ($>5\times10^{-3}$ cm^2/V) should be selected. An alternative is to eliminate the guard ring in future coplanar grid designs. This will require some research, since in present designs the guard ring helps assure adequate low-energy performance.

ACKNOWLEDGEMENTS

This work was funded by NASA's Planetary Instrument Definition and Development Program and by the Department of Energy Office of Safeguards and Security and Office of Nonproliferation Research and Engineering under contract W-7405-ENG-36.

REFERENCES

1. T. H. Prettyman, K. D. Ianakiev, C. E. Moss, et al., "Development of high efficiency, multi-element CdZnTe detectors for portable measurement applications," Los Alamos National Laboratory document LA-UR-00-1770, to appear in Journal of Radioanalytical and Nuclear Chemistry (2000).

2. Z. He, G. F. Knoll, D. K. Wehe, and Y. F. Du, "Coplanar grid patterns and their effect on energy resolution of CdZnTe detectors," Nuclear Instruments and Methods in Physics Research A, v. 411(#1), pp. 107-113 (1998).

3. T. H. Prettyman, K. D. Ianakiev, S. A. Soldner, and Cs. Szeles, "Effect of differential bias on the transport of electrons in coplanar grid CdZnTe detectors," Los Alamos National Laboratory document LA-UR-00-2875, submitted to Nuclear Instruments and Methods in Physics Research A (2000).

4. T. H. Prettyman, M. K. Smith, and S. A. Soldner, "Design and characterization of cylindrical CdZnTe detectors with coplanar grids," Proceedings of SPIE, Vol. 3768, pp. 339-347 (1999).